“Hidden” CO_2 in Amine-modified Porous Silicas Enables Full Quantitative NMR Identification of Physi- and Chemisorbed CO_2 Species

*Ricardo Vieira†, Ildefonso Marin-Montesinos†, João Pereira, Rita Fonseca, Marina Ilkaeva, Mariana Sardo, Luís Mafra**

*lmafra@ua.pt

CICECO – Aveiro Institute of Materials, Department of Chemistry, University of Aveiro, Campus Universitário de Santiago, 3810-193 Aveiro, Portugal

KEYWORDS

CO_2 adsorption, solid-state NMR, amine-modified mesoporous silicas, CO_2 quantification, chemical shift anisotropy, longitudinal relaxation time (T_1)

ABSTRACT

While spectroscopic investigation of surface chemisorbed CO_2 species has been the focus of most studies, identifying different domains of weakly interacting (physisorbed) CO_2 molecules in confined spaces is less trivial as they are often indistinguishable resorting to (isotropic) NMR chemical shift or vibrational band analyses. Herein we undertake for the first time a thorough solid-state NMR analysis of CO_2 species physisorbed prior to and after amine-functionalization of silica surfaces; combining ^{13}C NMR chemical shift anisotropy (CSA) and longitudinal relaxation times ($\mathbf{T_1}$). These methods were used to quantitatively distinguish otherwise overlapping physisorbed CO_2 signals, which contributed to an empirical model of CO_2 speciation for the physi- and chemisorbed fractions. The quantitatively measured $\mathbf{T_1}$ values confirm the presence of CO_2 molecular dynamics on the microsecond, millisecond and second time scales, strongly supporting the existence of up to three physisorbed CO_2 species with proportions of about 15%, 15% and 70%, respectively.

Our approach takes advantage from using adsorbed ^{13}C-labelled CO_2 as probe molecules and quantitative cross-polarization magic-angle spinning to study both physi- and chemisorbed CO_2 species, showing that 45% of chemisorbed CO_2 versus 55% of physisorbed CO_2 is formed from the overall confined CO_2 in amine-modified hybrid silicas. A total of six distinct CO_2 environments were identified from which three physisorbed CO_2 were discriminated, coined here as 'gas, liquid, and solid-like' CO_2 species. The complex nature of physisorbed CO_2 in the presence and absence of chemisorbed CO_2 species is revealed, shedding light on what fractions of weakly interacting CO_2 are affected upon pore functionalization. This work extends the current knowledge on CO_2 sorption mechanisms providing new clues towards CO_2 sorbent optimization.

1. INTRODUCTION

The International Panel on Climate Change (IPCC) predicts that in 2100 the concentration of CO_2 in the atmosphere will be about 570 ppm, which will promote an increase of 1.5 °C in the average atmospheric temperature.[1] The use of solid sorbents for post-combustion capture of CO_2 from flue gas[2–4] is considered one of the most effective approaches to mitigate anthropogenic CO_2 emissions, having many advantages over the decades-old amine CO_2 scrubbing technology, including their potential for a more cost-efficient regeneration and more environmentally sustainable solution compared to aqueous amines. Among many sorbent contenders towards this aim, amine-modified porous silicas have been the target of immense research as they possess relevant properties (*e.g.*, moisture tolerance, ability to chemisorb dilute CO_2 from gas mixtures) necessary for post-combustion CO_2 capture applications. The ability to tailor the chemistry of this class of porous sorbents through surface functionalization provides an exceptional testing ground whereby CO_2 speciation in confined spaces can be studied by vibrational[5–8] and NMR[9–17] spectroscopies. These atomic scale studies will ultimately provide feedback on structure-property relationships, *i.e.*, how distinct CO_2-adducts affect key sorbent properties such as CO_2 adsorption capacity, selectivity, among others, in relevant gas mixtures such as CO_2/N_2,[18,19] CO_2/CH_4,[19,20] with a large socio-economic impact.

It has been shown that various chemisorbed CO_2 species are formed in amine-modified mesoporous silica[5,9–12] and MOF[21–24] materials upon CO_2 adsorption. In particular, our group was able to identify three distinct types of CO_2-adducts (e.g., carbamic acid, alkylammonium carbamate) formed upon reaction of CO_2 with amine molecules possessing distinct bulkiness/nucleophilicities, combining solid-state (ss) NMR and computer modeling.[9–12] Chemisorbed CO_2 species are clearly distinguished via ^{13}C ssNMR appearing at chemical shifts

above 150 ppm.[9–12] Various infra-red (IR) spectroscopic studies were also able to distinguish different species of chemisorbed CO_2, from which some authors tentatively assigned these CO_2 species to ammonium carbamate, silylcarbamate, and free carbamic acid.[5–8] Additionally, a detailed analysis of CO_2 adsorption energetics over amine-functionalized mesoporous silica by DFT modeling to clarify the capture mechanism was performed providing a theoretical basis for carbamic acid and carbamates species formation.[25]

Although physisorbed and free CO_2 species only contribute with a single prominent resonance in the ^{13}C NMR spectrum at *ca*. 125 ppm, two different vibrational modes have been identified in the mesoporous silica SBA-15 via IR spectroscopy: one corresponding to CO_2 species vibrating in gas-like conditions, and another associated to hydrogen bonded CO_2 to silanol groups.[5] Upon SBA-15 amine-functionalization, the distinction between different types of physisorbed CO_2 species is no longer possible via IR.

Gas physisorption in porous silica has also been studied using small-angle neutron scattering (SANS). Chiang, W.-S. *et al*., showed that two layers of physisorbed CH_4 adsorbed on SBA-15, differing in density, can be detected by SANS being the layer closer to the surface of a liquid like density and the center layer having a vapor-like density.[26] This technique is nevertheless limited to hydrogen-containing gases and does not quantify the amount of gas of different layers. Computer simulations of N_2 adsorption on SBA-15 also provided evidence for the existence of two different density layers of N_2.[27]

The ability to quantify CO_2 species with variable adsorption strengths (e.g., chemisorbed and physisorbed) is very important to tailor sorbent materials for different target industrial applications wherein a specific type of adsorption mechanism may have, for instance, an impact on sorbent

regeneration. Despite the difficulties associated with IR quantification studies because the silica support is not transparent to IR, attempts to quantify either chemisorption or physisorption CO_2 species have been made, assuming the relation between the area under the physisorbed band and the amount of physisorbed CO_2 is unaffected when calcined and amine-modified SBA-15 are compared.[5]

Tracking distinct physisorbed CO_2 environments quantitatively using chemical shifts, NMR's most ubiquitous parameter, is not of much help, unless the adsorbed gas molecule has a distinctive chemical shift from the free gas in the sample holder. This is unfortunately not the case of CO_2 adsorbed in silica sorbents. To our knowledge, *distinct* physisorbed species have not been yet detected using ssNMR, despite of the high versatility and discrimination power of the technique. In this work, we reveal unprecedented details about the structure of physisorbed CO_2 in SBA-15 and its amine-modified analogue. We show, for the first time, that ssNMR can straightforwardly distinguish and quantify up to three distinct physisorbed CO_2 species using a combination of ^{13}C NMR chemical shift anisotropy and NMR relaxation measurements. Based on our spectroscopic observations, we propose a tentative model for the distribution of the distinct physically and chemically adsorbed CO_2 species in the material's channels.

Prof. Michael Hunger dedicated a great part of his scientific career to study the local structure of acid sites at the surface of porous solids (mostly zeolites) using probe molecules.[28] Additionally, he pioneered the use of flow-MAS NMR methods[29] for in-situ studies of porous catalysts. Our contribution also deals with the use of probe molecules (^{13}C-labeled CO_2), but this time to study the structure of CO_2 species formed at the surface of porous silicas. This work is our tribute to him; his work has been a great source of inspiration not only to our NMR group but also to many other researchers around the globe.

2. METHODS

2.1. Materials preparation

SBA-15 was synthesized according to a procedure reported previously by our group.[9] Firstly, $(EO)_{20}(PO)_{70}(EO)_{20}$ copolymer (4.0 g; Aldrich) was dissolved in a 1.6 M solution of HCl (126 cm^3). Next, tetraethyl orthosilicate (TEOS; 9.1 cm^3; Aldrich) was added to this solution with constant stirring. The solution was then stirred at 40 °C for 20 h and subsequently heated at 100 °C for 24 h, under static conditions. Afterwards, the solution was filtered and the obtained solid was washed with deionized water and dried in an oven at 40 °C. The solid (**as-synthesized SBA-15**) was calcined at 550 °C for 5 h with a heating ramp of 1°C/min. The resulting SBA-15 (**calcined SBA-15**) product was stored in a desiccator for further use.

Calcined SBA-15 was functionalized with a primary amine, 3-aminopropyltriethoxysilane (APTES) (*Sigma-Aldrich*, purity >98%). 2 g of SBA-15 were introduced in a closed reflux apparatus connected to a vacuum line and heated to 150 °C for 2 h. After cooling, nitrogen was introduced into the system prior to the opening of the reflux apparatus, and SBA-15 was refluxed with 100 cm^3 of dry toluene (*Alfa Aesar*, 99.8%) containing 9 mmol of APTES for 24 h in a nitrogen atmosphere. The resulting material (**APTES@SBA-15**) was purified by Soxhlet extraction with dry toluene, to remove the unreacted amino-alkoxysilane, and finally dried under vacuum, at 120 °C for 24 h.

2.2 $^{13}CO_2$ sorption procedure

The sorption apparatus comprises a laboratory-made high-vacuum line, connected to a turbomolecular pumping station (*HiCube 80, Pfeiffer Vacuum*), capable of vacuum greater than

10^{-2} Pa. A borosilicate glass cell was connected to the vacuum line and served as an enclosure for an NMR rotor to allow degassing and heating zirconia NMR rotors up to 300 °C under high vacuum. The heating was performed with a laboratory-made oven connected to a power controller (*Eurotherm 3116*), and the temperature measured with a thermocouple. The desired gas was introduced into the system from the canister connected to the vacuum line and the cell. The pressure inside the cell was measured with a capacitance transducer (*MKS instruments, Baratron 722B*).

All samples of APTES@SBA-15 were packed in zirconia NMR rotors, enclosed into the sorption apparatus, and dried by degassing and heating (150 °C, 3 h, ramp of 2.5 °C/ min) under vacuum. After cooling down under vacuum, $^{13}CO_2$ (*Cortecnet*, 99 atom % ^{13}C; < 3 atom % ^{18}O) was introduced into the system at a partial pressure of 770 Torr and allowed to equilibrate for 4.5 h. Finally, the NMR rotor was closed inside the cell and only then the cell was opened to remove the rotor for NMR measurements.

2.3 Chemical and morphological characterization

2.3.1. Electron microscopy

A high-resolution energy-filtered transmission electron microscope – HR-(EF)TEM, *JEOL* model *2200FS*, equipped with a scanning system, was used to image the samples at an acceleration potential of 200 kV. Preparation of the specimens consisted of suspending approximately 2 mg of the mesoporous silica powder in 2 mL of pure ethanol inside a 2 mL centrifuge tube. The mixture was agitated in a vortexer for 1 min, sonicated in a bath for 20 seconds and further agitated for 5 min. Then a droplet (from a Pasteur pipette) of the suspension was applied on the formvar-coated side of a *Ted Pella* Carbon Type-A 300 mesh copper grid. After solvent evaporation, the grids were

left in a desiccator with $CaCl_2$ until observation. The representative micrographs obtained are presented as Supporting Information.

2.3.2. N_2 adsorption porosimetry

Brunauer–Emmett–Teller specific area (BET) and *Barrett–Joyner–Halenda* porosimetry (BJH) measurements were achieved using the *Quantachrome–Autosorb IQ2* gas sorption analyzer. All samples were degassed under dynamic vacuum at 100 °C for 4 h (heating at a rate of 5 °C per minute). The complete N_2 adsorption/desorption isotherms at 77.300 K are presented in the Supporting Information.

2.3.3. Powder X-Ray Diffraction

The powder diffractograms of all materials were obtained through a *Malvern Panalytical Empyrean* diffractometer (Copper K-α radiation) using a small-angle X-ray scattering (SAXS) rotating window with mylar film as a support.

2.3.4. Infrared spectroscopy

A *Mattson Instruments GALAXY SERIES FT-IR 7000* spectrometer was used for infrared spectroscopy (IR). The samples were prepared by the KBr pellet method. The dried silicas were milled in an agate mortar with dried KBr (both dried under dynamic high vacuum overnight at 100°C). The powder was then pressed into a 2 mm pellet under 10 tons for 5 minutes.

2.3.5. Elemental Analysis

A *Truspec 630-200-200* CHNS analysis instrument was used for elemental analysis. The combustion furnace temperature was 1075 °C, with the afterburner at 850 °C. Quantification of C,

H and S used IR absorption; N was quantified by thermal conductivity. Raw values of all replicas are provided in **Table S1**.

2.4. Solid-State NMR spectroscopy

Single pulse (**Fig. 1a**), conventional CP (**Fig. 1b**) and Multiple Cross Polarization (**MultiCP, Fig 1c**) ^{13}C NMR spectra were acquired on a *Bruker Avance III 400* spectrometer operating at B_0 field of 9.4 T, with ^{13}C Larmor frequency of 100.6 MHz. The $^{1}H–^{13}C$ heteronuclear correlation (**HETCOR**) NMR spectrum was registered in a Bruker Avance III 700 operating at B_0 field of 16.4 T, with ^{13}C Larmor frequency of 176.05 MHz. All experiments were performed on a double-resonance 4 mm Bruker magic-angle spinning (**MAS**) probe.

MultiCP experiment used a total of n=6 CP blocks, fulfilling the *Hartmann-Hahn* condition at the radio frequency (RF) field strengths of 55 kHz in the ^{13}C channel and 48 kHz in the ^{1}H channel with a contact time ($\mathbf{CT_2}$) of 15 μs. The ^{1}H RF field has a ramped-amplitude from 90% to 100%. The recycle delay ($\mathbf{D_1}$), inter-CP-blocks delay ($\mathbf{D_2}$) and MAS frequency were respectively 7.5 s, 3 s, 10 kHz for **Fig. 2** and 2.5 kHz for **Fig. 3a** and **Fig. 4a**. In the single pulse MAS experiment $\mathbf{D_1}$ and MAS frequency were respectively 250 s and 10 kHz, the ^{13}C $\pi/2$ pulse length was 6 μs using a RF field strength of 42 kHz. Conventional CP measurements used $\mathbf{D_1}$ of 7.5 s with a contact time ($\mathbf{CT_1}$) of 3 ms and power of 55 kHz pulse in the carbon channel and a 48 kHz pulse in the proton channel, with a RF ramped-amplitude from 50% to 100%. For all the above experiments, ^{1}H decoupling was applied during acquisition using SPINAL-64 decoupling using at RF field strength of 70 kHz. The fitting of the MultiCP and MAS spectra was performed with DMFIT.[30] The obtained parameters are shown in **Tables S2** and **S3**.

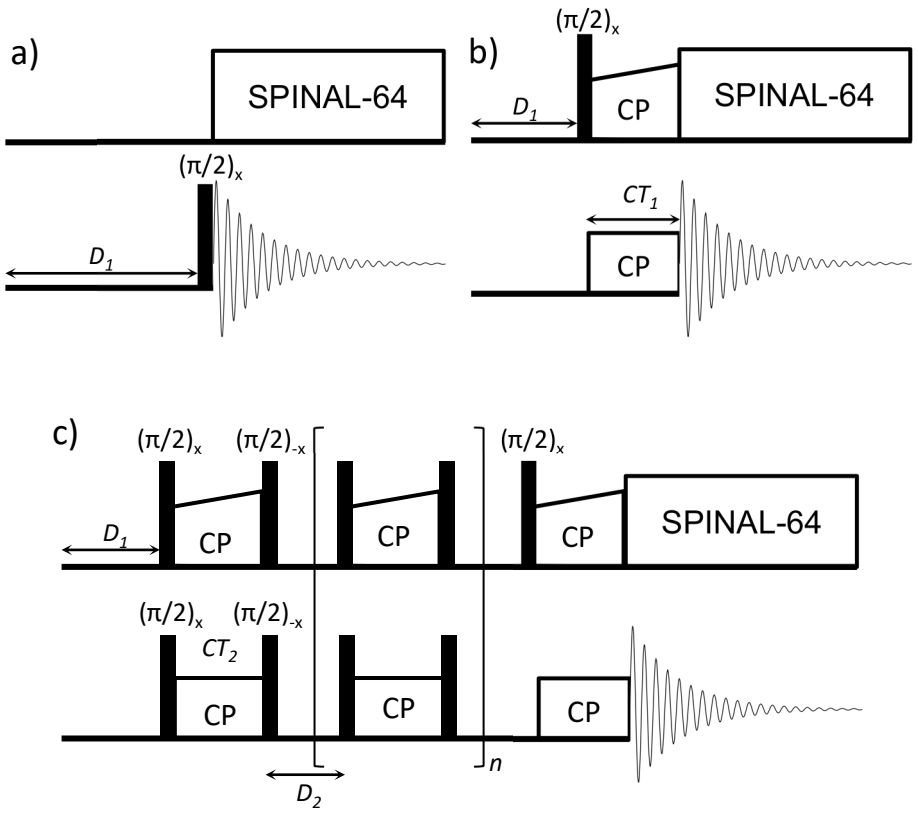

Figure 1 - Schematic for pulse sequences a) single pulse; b) conventional cross polarization; c) multiple cross polarization, to record the ^{13}C MAS NMR spectra shown in Fig. 2. The abbreviatures and acronyms used in this figure are defined in subsection 2.4, Solid-State NMR spectroscopy.

Longitudinal relaxation times ($\mathbf{T_1}$) were measured with a saturation-recovery pulse sequence[31] (**Fig. S4**) at MAS rates of 10 kHz with a ^{13}C π/2 pulse length of 4.5 μs using a RF field strength of 55 kHz and magnetization recovery times, t. ranging from 0.5 μs to 30 s (**Table S5**). The restoration of nuclear magnetization is fitted using the following exponential model:

$$M_z = \sum_{i=1}^{n} M_{0,i}\left(1 - e^{-\frac{t}{T_{1,i}}}\right)$$

Where $\boldsymbol{M_z}$ is the total magnetization along z-axis, $\boldsymbol{M_{0,i}}$ is the magnetization at thermal equilibrium of each ^{13}C resonance $\boldsymbol{i}$, corresponding to the quantity of the distinct CO_2 species; and $\boldsymbol{T_{1,i}}$ is the longitudinal relaxation time of each $^{13}CO_2$ species $\boldsymbol{i}$.

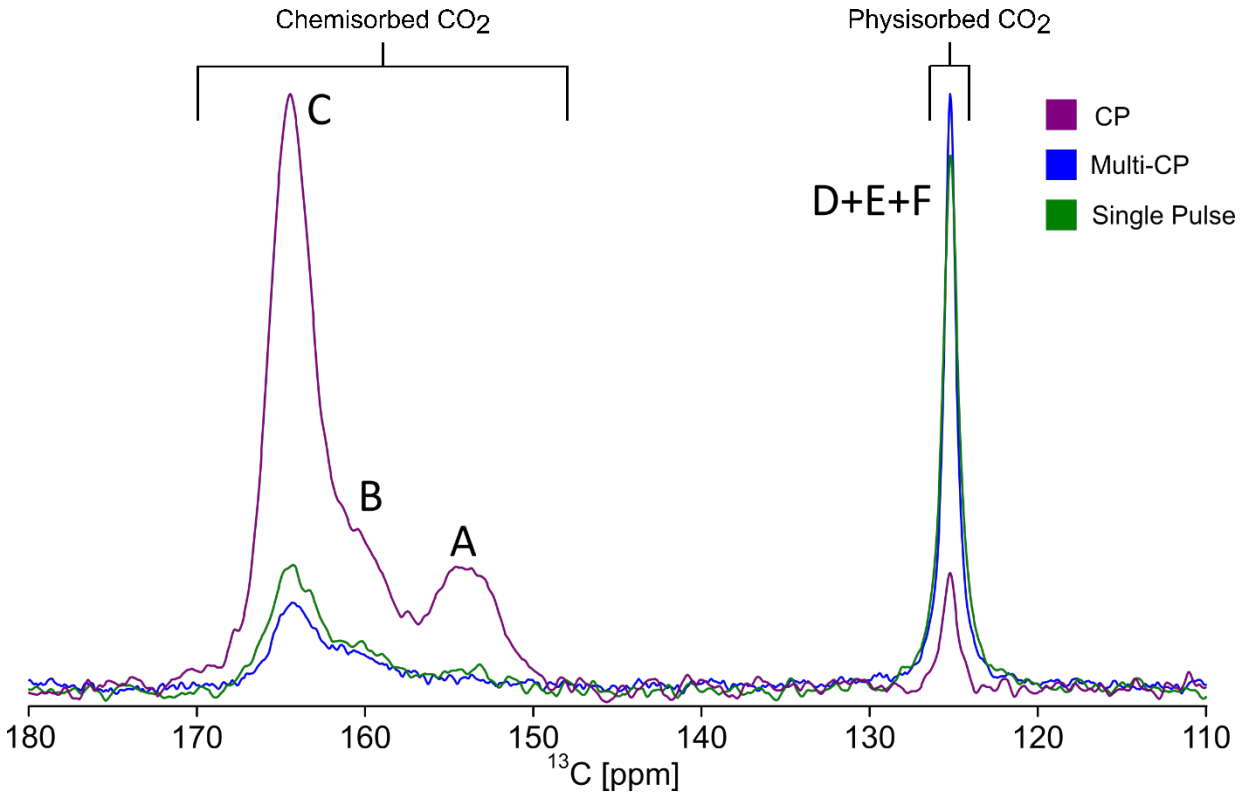

Figure 2 - ^{13}C-NMR spectra of APTES@SBA-15 at 9.4 T after adsorption of $^{13}CO_2$ (P=770 Torr) using three different NMR pulse sequences (as indicated by the different colors) to compare their quantitative performance. The contact time for conventional CP and the MultiCP were 3 ms and 15 μs, respectively. The conventional CP and the MultiCP NMR spectra were both acquired using 256 scans corresponding to acquisition times of 35 minutes and 4 hours respectively. The single pulse spectrum was acquired using 1024 scans (acquisition time of 71 hours) to normalize the signal-to-noise ratio of all the three pulse sequences experiments and obtain comparable signal intensities. CO_2 chemisorbed and physisorbed species are identified as A, B, C and D, E, F, respectively.

Refocused transverse dephasing times ($\mathbf{T_2^*}$) were measured using a spin-echo pulse sequence at MAS frequency of 10 kHz. The ^{13}C π/2 and π pulse lengths were 8.5 μs and 17 μs, respectively using a RF field strength of 29.4 kHz. The transverse magnetization recovery times (t) ranging from 1 μs to 200 ms (**Table S6**) and the $\mathbf{D_1}$ was set to 15s. The decay of the transverse nuclear magnetization is fitted using the following exponential model:

$$M_{xy}(t) = \sum_{i=1}^{n} M_{xy,i}^{0}\, e^{-\frac{t}{T_{2,i}^{*}}}$$

Where $M_{xy}(t)$ is the total transverse magnetization at a time t, $M_{xy,i}^{0}$ and $T_{2,i}^{*}$ are the initial transverse magnetization and the refocused transverse dephasing time of each $^{13}CO_2$ species i, respectively.

The ^{1}H–^{13}C HETCOR NMR spectrum of $^{13}CO_2$/APTES@SBA-15 was acquired at 16.4 T using frequency-switched Lee–Goldburg (FSLG) ^{1}H homonuclear decoupling during the indirect dimension (t_1). Lee-Goldburg (LG)-CP was employed to achieve ^{1}H to ^{13}C magnetization transfer. ^{13}C rf amplitude ramped at 50–100%, and a rf amplitude for ^{1}H spin-lock of 50 kHz at a LG offset irradiation of $-50000/\sqrt{2}=-35354$ Hz. 50 t_1 points with 1.5k scans each were recorded along the indirect dimension. A ^{1}H rf field strength of 83 kHz and asymmetric LG offsets of 54 925 Hz and –62 925 Hz were used for FSLG decoupling employing a LG pulse of 9.8 μs. The indirect dimension dwell time was set equal to four FSLG blocks (78.4 μs). Quadrature detection in t_1 was achieved by the States-TPPI method. The ^{1}H chemical shifts were corrected assuming a scaling factor of $1/\sqrt{3}$ for FSLG decoupling.

3. RESULTS AND DISCUSSION

3.1. Materials characterization

The results regarding materials characterization are summarised in the **Table 1**. TEM images (**Fig. S7**) and powder SAXS (**Fig. S8**) data are typical of an SBA-15 type material. SAXS study reveals the common pattern with the (100), (110), and (200) reflections of the hexagonal pore array of

SBA-15.[32] The N_2 sorption isotherms (**Fig. S9**) are all of type **IV** with **H1** hysteresis loops,[33] characteristic of materials with cylindrical mesopores with a mean pore diameter of approximately 7.6 nm. As expected, upon functionalization the grafted aminopropyl groups occupy significant amount of the pore volume halving the BET surface area. The BJH pore volume also decreases to 73%. The FTIR spectrum (**Fig. S10**) and the C/N ratio of *ca*. 3, estimated from elemental analysis (**Table S1**), suggest the presence of incorporated amines in the functionalized sample. From the nitrogen content and the calcined material's surface area we have obtained a surface density of *ca*. 1.2 grafted amines per nm^2.

***Table** 1 Overview of the textural, structural properties and chemical composition analysis results of the calcined and functionalized samples.*

	BET surface area /$m^2 \cdot g^{-1}$	**Pore volume[a] /$cm^3 \cdot g^{-1}$**	**Pore diameter[a] /nm**	**Lattice parameter[b] /nm**	**N content[c] /$mmol \cdot g^{-1}$**	**C content[c] /$mmol \cdot g^{-1}$**
calcined SBA-15	646	0.88	7.588	10.68	n/a	0.1443
APTES@ SBA-15	296	0.65	7.590	11.04	1.304	4.170

[a]*From the BJH analysis of the isotherm adsorption branch*
[b]*From the SAXS (100) reflection*
[c]*From the elemental analysis*

3.2. NMR strategies for quantifying physi- and chemisorbed CO_2

The NMR identification and quantification of adsorbed CO_2 species in porous materials entail two main difficulties:

1. Some of the CO_2 species are very diluted over the whole sorbent porous surface. Therefore, standard CP-MAS technique is needed to enhance the ^{13}C NMR signal of adsorbed CO_2, despite its non-quantitative nature.

2. Longitudinal relaxation times are usually much larger for chemisorbed CO_2 species than for physisorbed CO_2 in APTES@SBA-15 material (as shown in **Table S11** and **Table S12**). That leads to longer experimental times to acquire ^{13}C NMR spectra.

To limit the impact of these factors, and obtain NMR spectra with the highest possible sensitivity also providing quantitative information, the Multi-CP enhancement method described by Johnson and Schmidt-Rohr,[34] (**Fig. 1c**) was employed, for the first time in the context of studying CO_2 speciation. This technique enables homogenous $^{1}H \rightarrow ^{13}C$ magnetization transfer thus providing quantitative ^{13}C NMR spectra (**Fig. 2**), while maintaining the advantages of conventional CP (i.e., short recycling delays). This method reduced the measurement time of NMR spectra by a factor of ~3 showing a 4% difference in resonance intensity compared with ^{13}C direct excitation NMR experiments (*cf*. **Fig. 2**), which is in good agreement with previous reports.[34,35] Conventional single pulse ^{13}C MAS NMR must be used in the calcined SBA-15 as CP-based experiments were not efficient to detect physisorbed CO_2 at *ca*. 125 ppm due to its high mobility in samples lacking amine functionalization. Slow-MAS/Multi-CP ^{13}C NMR experiments were employed to extract the principal components of the ^{13}C CSA tensor, which allowed not only the detection but also the accurate quantification of the 'hidden' physisorbed CO_2 species (to be discussed ahead). Finally, ^{13}C $\mathbf{T_1}$ relaxation measurements were performed using saturation-recovery experiments to probe the molecular dynamics of the different CO_2 environments detected. As seen from **Fig. 3, 4** and **5**, the NMR approaches, employed in this work, complement each other, providing a unique toolbox for unambiguous identification and quantification of different CO_2 species otherwise impossible to assess without combining chemical shift analysis with relaxation and CSA measurements.

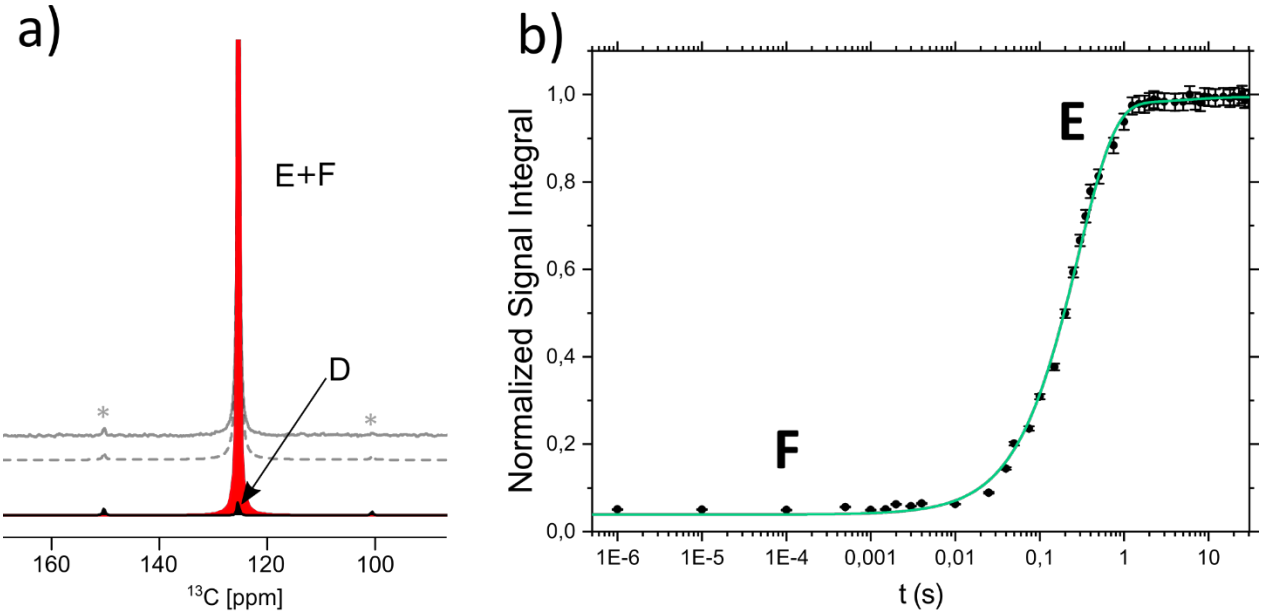

Figure 3 – a) Single pulse ^{13}C NMR spectrum of calcined SBA-15 recorded at a MAS frequency of 2.5 kHz and at 9.4 T. Solid gray line is the experimental result, dashed line is the fitting. Black and red represent the different physisorbed CO_2 species (D and E+F), respectively. b) Plot showing the variation of the integral of the physisorbed peak over the magnetization recovery times contain in Table S5 using the saturation-recovery pulse sequence (Fig. S4). Green line is the fitted curve described in the text.

3.3. Detecting 'hidden' physisorbed CO_2 species

Fig. 3a and **4a** depict the experimental (solid gray line) and simulated (dashed gray line) ^{13}C NMR spectra of CO_2-adsorbed SBA-15 prior to and after amine-functionalization, respectively, along with the full spectral deconvolution. An intense resonance at *ca.* 125 ppm with a pair of small first order spinning sidebands is observed in the ^{13}C NMR spectrum. Nevertheless, this resonance could not be fitted using a single-site CSA model, due to the large discrepancy in intensities between the central peak and the spinning sidebands. It becomes clear that a second component contributes to the intensity of this resonance, assigned to the physisorbed CO_2 species. Therefore, the peak at *ca.*

125 ppm was fitted using a two-component model, one accounting for the component originating spinning sidebands, designated **D** (**Fig. 3a**, **4**, **5a**, black component, and another dominant component comprising species **E+F**, which do not yield spinning sidebands (**Fig. 3a**, **4**, and **5a**, red component). Although **E** and **F** resonances overlap due to their identical chemical shifts, they can be distinguished based on their different $\mathbf{T_1}$ relaxation times as both resonances correspond to dynamically distinct CO_2 species (*cf*. **Fig. 3b**, **4** and **5b**).[36]

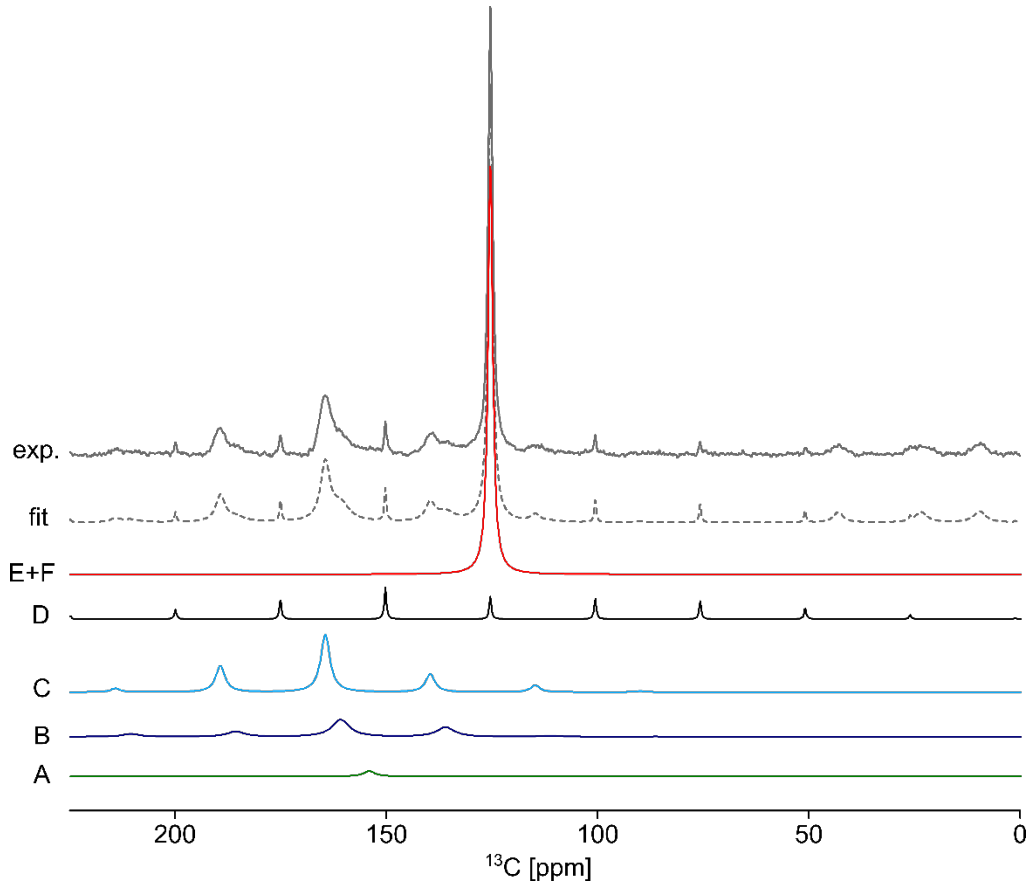

Figure 4 – MultiCP ^{13}C NMR spectrum of APTES@SBA-15 after adsorption of $^{13}CO_2$ (P = 770 Torr) acquired at 9.4 T with a contact time of 15 µs. Solid gray line at the top is the experimental spectrum, dashed line is the fitting. Green, dark blue, light blue correspond to the fitted chemisorbed components A, B and C. Black and red represent the fitted physisorbed components D and E+F species.

For the calcined SBA-15 sample, the measured $\mathbf{T_1}$ build up curve shows that two different components **E** and **F** can be separated. Component **F** appears fully recovered already at the lowest time value of *ca*. 0.5 ms (**Fig. 3b**). We therefore estimate a $\mathbf{T_1}$ in the microsecond scale for CO_2 species **F**, whereas a much larger $\mathbf{T_1}$ relaxation time, in the millisecond range, was obtained for the CO_2 species **E**. It is worth mentioning that the resonance associated with species **D**, observed in the MultiCP NMR spectrum (**Fig. 3a**), could not be extracted from the $\mathbf{T_1}$ measurements likely due to its weak intensity thus hindering the detection thereof. Given the existence of a measurable CSA associated to **D**, which is typically the case of more rigidly adsorbed CO_2 molecules strongly interacting with the surface, this relaxation component is expected to yield ^{13}C $\mathbf{T_1}$ in the order of seconds.[37] The unambiguous assignment of **D** to strongly interacting CO_2 species will, however, only become apparent in the discussion that follows.

On the other hand, the measured $\mathbf{T_1}$ build up curve of the amine-functionalized silica sample identifies three different components. Again, component **F** whose magnetization is fully recovered already at the lowest magnetization recovery time of 0.5 ms, the larger component **E** ($\mathbf{T_1}$ = 90 ms), also observed in the calcined SBA-15 sample, and a third (new) component assigned to CO_2 species **D**, showing the largest value ($\mathbf{T_1}$ = 2.4 s, **Table S12**). Quantification of all detected physisorbed CO_2 species by CSA and T_1 analyses are listed in **Tables S2** and **S12** for comparison. Notice that the quantity of species **D** is now measurable (about 15% of the total amount of physisorbed CO_2 species) in APTES@SBA-15 as compared with calcined SBA-15 (*cf*. **Fig. 4b** and **3b**). Comparing the quantities of physisorbed CO_2 species presented in **Table S12**, one can conclude that CO_2 species **D**, showing the largest $\mathbf{T_1}$ value, corresponds indeed to the resonance at *ca*. 125 ppm shown in black colour (**Fig. 5a**), also labelled as **D** for the sake of comparison. This can be validated by the very similar quantifications of **D**, retrieved from ^{13}C MultiCP NMR spectral

deconvolution (**Fig. 5a**) and $\mathbf{T_1}$ curve fitting (**Fig. 5b**), amounting to 13% and 15%, respectively. This 2% difference is within error.

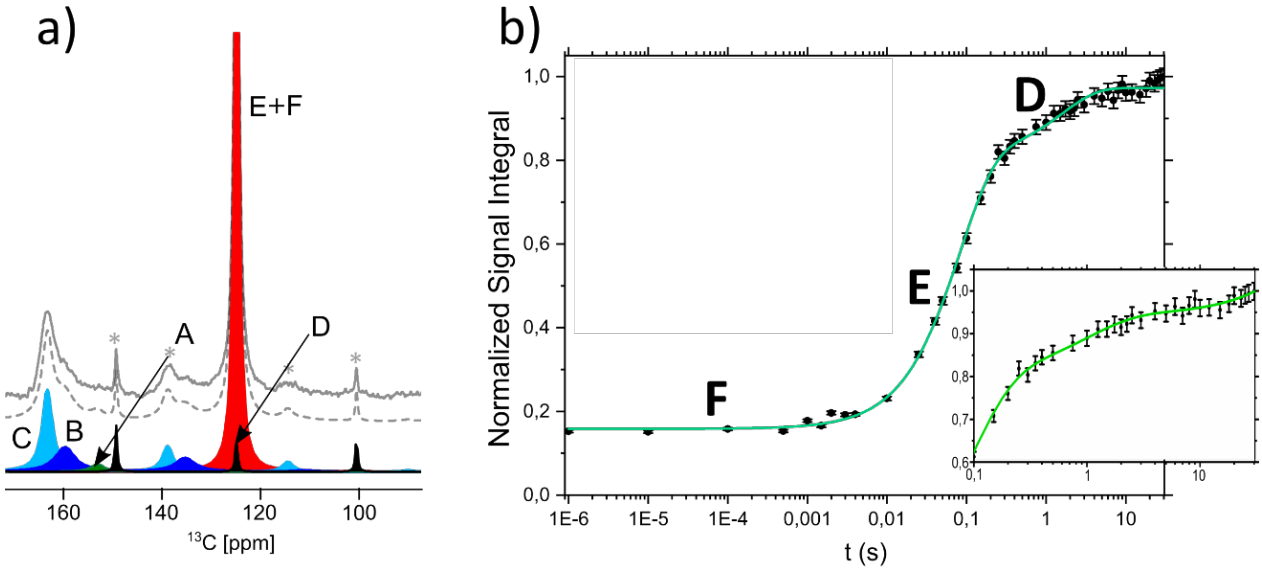

*Figure 5 – a) A magnified detail of the MultiCP ^{13}C NMR spectrum of APTES@SBA-15 showed in **Fig. 4**. Solid gray line is the experimental spectrum, dashed line is the fitting. Green, dark blue, light blue, black and red represent the different A, B, C, D and E+F species, respectively. b) Plot showing the variation of the ^{13}C peak integral (~ 125 ppm) of the physisorbed CO_2 over the magnetization recovery times listed in Table S5 using the saturation-recovery pulse sequence (Fig. S4). Green line is the fitted curve described in the text. The inset at the lower right shows a detailed portion of the plot.*

To summarize, we have combined ^{13}C NMR (including CSA analysis) and ^{13}C $\mathbf{T_1}$ measurements to separate three distinct CO_2 species in both calcined SBA-15 and APTES@SBA-15 (**Table 2**): the presence of a dominant **E** component and two smaller components **D** and **F** with integrated values of 3% (**D**) / 92% (**E**) / 5% (**F**) (**Fig. 3b** and **Tables 2 and S12),** and 15% (**D**) / 70% (**E**) / 15% (**F**) (**Fig. 5b** and **Table S12),** for calcined SBA-15 and APTES@SBA-15 samples, respectively. Additionally, the $\mathbf{T_1}$ values increase in the following order: $\mathbf{T_1}$(**D**) > $\mathbf{T_1}$(**E**) > $\mathbf{T_1}$(**F**), presenting different orders of magnitude between each other, *i.e.*, **D**, **E** and **F** T_1s are in the seconds,

milliseconds, and microseconds timescales, respectively. One can also relate $\mathbf{T_1}$ magnitudes with molecular rigidity. The larger is the $\mathbf{T_1}$, the higher is the CO_2 rigidity and the stronger are the CO_2-surface interactions. Therefore, we can assume **D** is the least mobile of the physisorbed species, showing a ^{13}C $\mathbf{T_1}$ that is comparable with solids, albeit our measured $\mathbf{T_1}$ values could also fit liquid phase media according to literature.[36,38] For instance, $\mathbf{T_1}$ measurements stemming from various amine solutions[38] give rise to values ranging from 0.4 to 10.2 s. In the case of species **E,** the measured $\mathbf{T_1}$ is compatible with molecular mobility in dense confined gas similar to what was observed in $^{13}CO_2$-adsorbed metal-organic frameworks, $Cu_3(btc)_2$ and $Cu_{3-x}Zn_x(btc)_2$, where $\mathbf{T_1}$ between 10 and 100 ms were obtained.[39] **F** is the most mobile CO_2 species showing the lowest $\mathbf{T_1}$ (<500 μs), which is in very good agreement with our $\mathbf{T_1}$ measurement of pure CO_2 gas (**Table S12**).

***Table** 2 Quantification of the relative fractions of the different CO_2 species present in the three studied mesoporous silica materials.*

	Chemisorbed			**Physisorbed**		
	A (%)	**B (%)**	**C (%)**	**D (%)**	**E (%)**	**F (%)**
APTES@SBA-15	2	16	27	8	39	8
calcined SBA-15	-	-	-	3	92	5
as-synthesized SBA-15	-	-	-	-	100	-

From these results, one can see that the population of CO_2 species **D** and **F** is augmented upon amine-functionalization at the cost of CO_2 species **E**. The increase in component **D** is most probably due to the increase in available hydrogen atoms to bond with, since component **D** is formed by physisorbed CO_2 strongly interacting with the surface, most likely due to silanol-CO_2

hydrogen bonding as proposed by IR[5] in SBA-15 and chemisorbed CO_2 – physisorbed CO_2 interactions in APTES@SBA-15.[10] We have acquired a $^{1}H–^{13}C$ LG-CP HETCOR spectrum (**Fig. 6**) to try obtaining a better insight into CO_2-surface interactions. This spectrum clearly shows the correlation (marked with orange dots) of the ^{13}C resonance corresponding to **D** (*ca*. 125 ppm) with three distinct ^{1}H resonances, corresponding to the proximity of physisorbed CO_2 to silanol and/or propylamine methylene groups (δ_H = 1.6 and 2.7 ppm) and possibly the amine moieties (δ_H = 7.3 ppm) stemming from grafted propylamine on the silica surface.

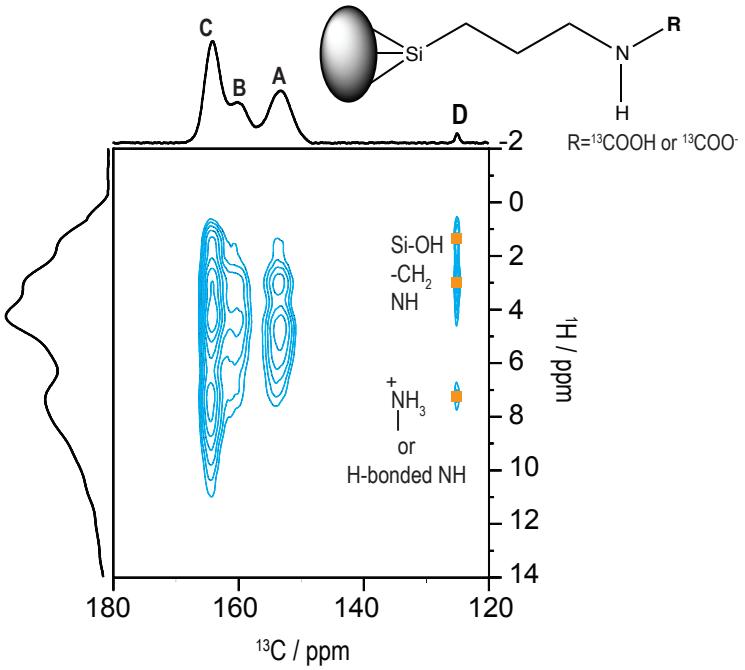

Figure 6 – $^{1}H–^{13}C$ HETCOR NMR spectrum of $^{13}CO_2$/APTES@SBA-15 recorded at 16.4 T using a contact time of 2 ms, 1536 scans and a total acquisition time of 640 minutes.

The rise in species **F** upon amine-functionalization is likely due to thermodynamic equilibrium. The increase in component **D** (dense layer) is compensated by increasing the layer with less density (**F**) in order to maintain the CO_2 pressure constant in both samples.

Different groups have previously carried out an extensive theoretical and experimental study of chemisorbed CO_2 structures in amine-modified silicas,[9,12,17,25] showing that the three chemically distinct species **A, B** and **C** are assigned to: i) isolated carbamic acid species possibly interacting on with surface silanol groups, ii) carbamic acid species interaction with two APTES groups and iii) formation of alkylammonium carbamate ion pairs, respectively. The quantitative analysis performed in this work, estimates relative proportions between species **A**, **B** and **C** of 2%, 16% and 27%, respectively (**Table 2** and **S2**)**.**

An estimation of CO_2 residing 'outside' the pores is a complicated task due to the inherent dilution of this fraction. However, we have undertaken a series of measurements with the aim of answering this question. We performed similar experimental measurements as mentioned above, but this time for as-synthesized SBA-15 (**Fig. S13**), which contains the organic structure directing agent (OSDA) molecules blocking the pores. Therefore, we expect that a small fraction of the CO_2 molecules interacts with the external surface of the silica particles, stay as bulk gas in the inter-grain regions or fill the empty spaces of the NMR rotor. The ^{13}C MAS NMR spectrum of as-synthesized SBA-15 shows a single peak at *ca*. 125 ppm with only 5% of the peak intensity of calcined SBA-15 (**Fig. S14**). So, one could be persuaded to assign that quantity to approximately the amount of CO_2 outside the mesopores, however our $\mathbf{T_1}$ (**Fig. S13**) and $\mathbf{T_2^*}$ measurements (**Table S15, Fig. S16, Fig. S17** and **Table S18**) do not support this hypothesis. Note that $\mathbf{T_1}$ measured on the as-synthesized SBA-15 sample showed only a single component in the millisecond timescale. This $\mathbf{T_1}$ value agrees with the one of species **E** observed in APTES@SBA-15 and calcined SBA-15 but is not compatible with the expected value of a bulk gas species with values, typically in the range of microseconds, further indicating that this species might be in contact with the silica surface or the OSDA molecules. The full width at half-maximum measured for the peak of CO_2

species **E** is the widest of all measured ones in the different species found in each material studied in this work. This is a clear indication of a fast $\mathbf{T_2}$ relaxation, likely induced by the rich ^1H environment supplied by the presence of OSDA molecules. The measured $\mathbf{T_2^*}$ also follows the same trend as the measured $\mathbf{T_2}$ values (**Table S15**). The presence of organic molecules is supported by elemental analysis (**Table S1**) and FTIR (**Fig. S10**, stretching band at 2978 cm^{-1} typical of CH_2 groups), evidencing that the content in organic components is the highest of all the samples. Our interpretation is that the observed $^{13}CO_2$ signal (**E**) in the as-synthesized SBA-15 might correspond to CO_2 adsorbed either at the pore entrance or in the accessible volume within the silica pores occupied with OSDA. Imperfections/defects in OSDA coverage can also create CO_2 adsorption sites. Moreover, the absence of a fast (microsecond) relaxation component in as-synthesized SBA-15 also supports that the species **F**, observed in the other samples might be due to CO_2 that is indeed present inside the pore channels. Nevertheless, we do not discard the possible presence of a small fraction of CO_2 species outside the channels, undetected due to the lack of NMR sensitivity.

3.4. Empirical Model of CO_2 distribution in amine-functionalized mesopores

The difference in $\mathbf{T_1}$ values can help elaborating a 'phenomenological' model of the CO_2 distribution within the silica cylindrical mesopores. As aforementioned, three physisorbed CO_2 species labelled **D, E** and **F** are detected in both calcined SBA-15 and APTES@SBA-15. In the latter material, up to three distinct $\mathbf{T_1}$ relaxation times were fitted from the magnetization recovery measurements (**Fig. 4b**), suggesting the presence of at least three dynamically distinct physisorbed CO_2 molecules. *Etesse* et al.[40] measured ^{13}C $\mathbf{T_1}$ relaxation in pure CO_2 gas and observed a direct relationship between CO_2 density (by increasing CO_2 pressure) and the ^{13}C $\mathbf{T_1}$ relaxation of CO_2. They observed that increasing CO_2 density leads to an increase of $\mathbf{T_1}$ values. We can thus infer that

species **D** pertains to denser domains than species **E**, which in turn is denser than species **F**, that is, ^{13}C $\mathbf{T_1}$ relaxation values decrease moving from the surface inwards. This observation also agrees with what has been proposed for confined CH_4 in SBA-15 silica by Chiang *et al*.[26]

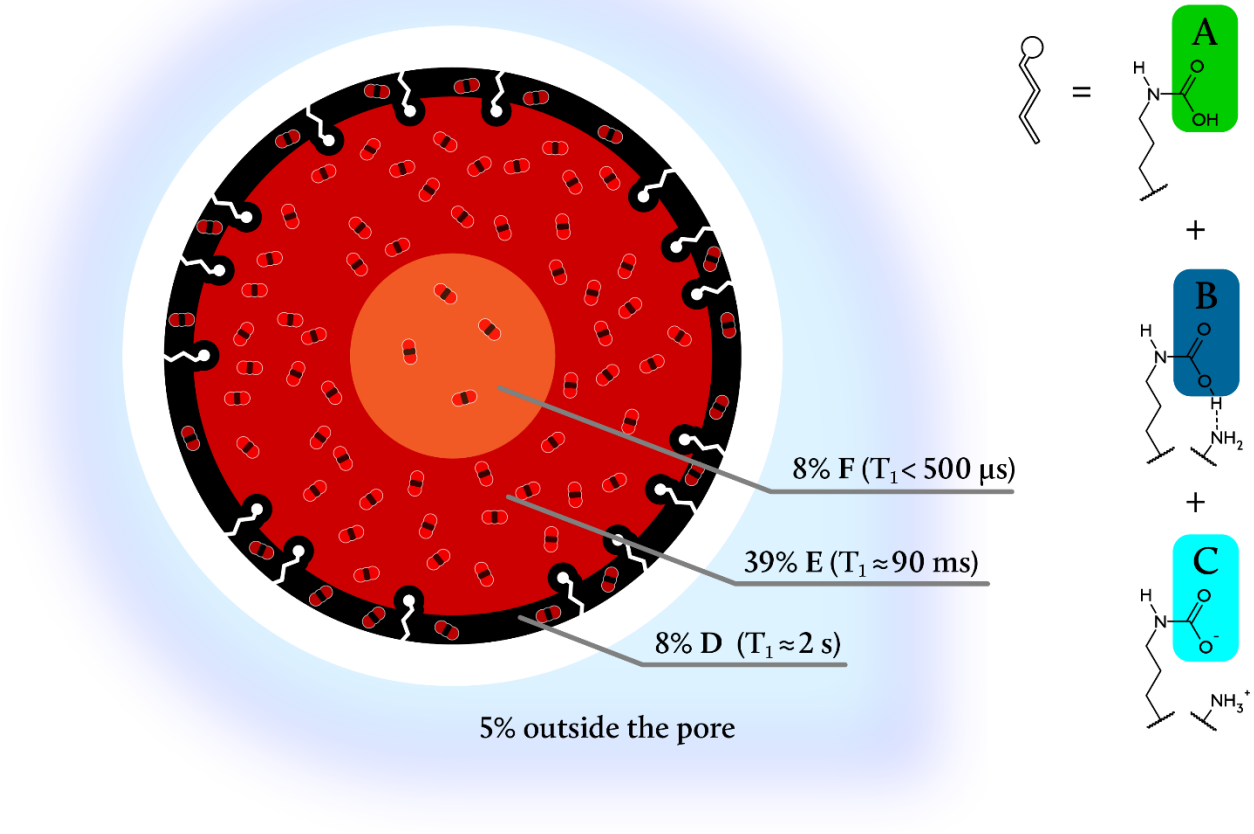

*Figure 7 - Schematic representation of a cylindrical mesopore functionalized with propylamine groups containing the six types of adsorbed CO_2species proposed in this work. Physisorbed species are represented in black (**D**), red (**E**) and orange (**F**), along with the corresponding quantification percentages and longitudinal relaxation times indicated in the legend. The chemical representation of the different chemisorbed species (**A**, **B** and **C**) is also displayed on the side. Chemisorbed CO_2 species are represented in white color.*

According to our interpretation of the data, we propose an empirical model for CO_2 distribution inside the APTES@SBA-15 channels as sketched in **Fig. 7** containing six different types of adsorbed CO_2 species (**Table 2**): 1) three chemisorbed CO_2 species, identified from ^{13}C MAS NMR spectra (**Fig. 2** and **Fig. 5a**) accounting for 45% of the total CO_2 present in the sample (2% **A**, 16% **B** and 27% **C**), and 2) three distinct physisorbed CO_2 species, summing up to 55% of the total CO_2 present in the sample (8% **D**, 39% **E**, 8% **F**). As mentioned earlier, species **D** is likely to be engaged in hydrogen bonding with the CO_2-adducts formed during chemisorption[10] and/or with silanol groups residing at the silica surface.[5] The remaining two CO_2 species (**E** and **F**) are similar as proposed by Chiang et al.[26], being **E** a liquid-like CO_2 layer deposited onto layer **D** and **F** tentatively assigned to a gas-like CO_2 state[26] located along the axis of the pore channel.

4. Conclusions

A novel NMR-based methodological approach has been designed to identify and quantify the multiple confined CO_2 species formed upon CO_2 adsorption in mesoporous materials. The combination of quantitative CSA analysis with Multi-CP and $\mathbf{T_1}$ longitudinal relaxation measurements reveals for the first time the nature of three distinct physisorbed CO_2 environments (**D, E, F**) in calcined SBA-15 and APTES@SBA-15 silica, impossible to distinguish resorting to ^{13}C chemical shift analysis, the most ubiquitous NMR parameter. This methodology has also been used for full quantification of six forms of CO_2 (**A-F**) detected in these porous materials, that is, the three different forms of chemisorbed CO_2 (**A, B, C**) encountered in our previous works,[9,11,12,41] plus the three physisorbed CO_2 species mentioned earlier. The relative proportions of the physisorbed CO_2 species are strongly related with the presence of chemisorbed CO_2 species in APTES@SBA-15. Particularly, CO_2 species **D** and **F** increase their relative proportions by 12% and 10%, respectively in the presence of chemisorbed species (cf. **Fig. 4**). The amount of these

two species is augmented, most likely, at the expense of curtailing species **E** by 22% with respect to the amount thereof in calcined SBA-15. These changes portray a chemically and thermodynamically interconnected complex system wherein three different physisorbed CO_2 species (**D, E, F**) depict very distinctive mobility environments as shown by their associated $\mathbf{T_1}$ relaxation values of 2 s (**D**), 0.2 s (**E**) and <500 μs (**F**). Interestingly, the quantification of chemisorbed and physisorbed species in APTES@SBA-15 stresses the importance of chemisorption in the design of optimal CO_2 solid porous adsorber media. The chemisorbed fraction is almost half (45%) of the total adsorbed CO_2 in APTES@SBA-15.

These observations allow us to propose an empirical CO_2 distribution model inside silica channels that highlight the complexity of the system (**Fig. 7**). Conventional adsorption models like Langmuir or BET consider that the adsorbate behaves as an ideal gas at isothermal conditions, assuming the surface to be homogeneous and the interactions between adsorbate molecules or between the adsorbates and the surface to be the same in all regions of the pore. It is well known that these approximations disregard relevant properties such as surface roughness and adsorbent/surface interactions.[42] Our experimental data is a first step towards unveiling the complexity of CO_2 physisorption in confinement showing that, at room temperature, there is not just a single interacting monolayer but multiple CO_2 domains of varying densities as a result of their distinct intermolecular interactions. This will therefore lead to differentiated motional behaviors pervading the pores.

We believe that the set of techniques and methodologies presented in this work could be used in general to identify and quantify trapped gas species in porous materials. Studies probing the effect of other grafted molecules into porous systems in the quantity of physi- and chemisorbed CO_2 species are underway. Understanding the nature of distinct CO_2 species formed and the type of

molecular mechanisms favoring the formation of both chemi- and physisorbed CO_2 species is therefore crucial to tailor sorbent materials towards improved gas separation. Moreover, accounting for physisorbed CO_2 species is extremely useful to generate more detailed atomistic models of CO_2 speciation upon adsorption of gases into porous materials, in contrast with more classical models. The information derived from these atomistic models is another direction we are taking and is expected to contribute to improve CO_2-adsorbent materials, helping to predict adsorption capacity and sorption/desorption kinetics of the adsorption processes.

AUTHOR CONTRIBUTION

† Ricardo Vieira and Ildefonso Marin-Montesinos have equally contributed to this work.

ASSOCIATED CONTENT

Supporting Information

The Supporting Information is available free of charge at:

Elemental analysis data, chemical shift anisotropy tensor conventions, chemical shift anisotropy analysis, saturation-recovery pulse sequence scheme, magnetization recovery times used to measure T_1, electron micrographs of calcine SBA-15, powder X-ray diffractograms, N_2 sorption isotherms, FTIR transmission spectra, ^{13}C T_1 relaxation times, single pulse spectrum of APTES@SBA-15 after adsorption of $^{13}CO_2$ and of as-synthesized SBA-15, normalized physisorbed peak signal intensity vs magnetization recovery times, comparison of ^{13}C NMR spectra of SBA-15 samples with and without template, table of the full width at half maximum and estimated T_2 and measured T_2^* relaxation times, bar plot of the T_2^* for each observed CO_2 species

in the different SBA-15 materials, the T_2 signal decay observed in the transverse dephasing refocused experiments and the fitted parameters for the T_2^* estimation.

ACKNOWLEDGMENT

This work was developed within the scope of the project CICECO-Aveiro Institute of Materials, UIDB/50011/2020 & UIDP/50011/2020, financed by national funds through the Portuguese Foundation for Science and Technology/MCTES. We also acknowledge funding from project PTDC/QUI-QFI/28747/2017 (GAS2MAT-DNPSENS - POCI-01-0145-FEDER-028), financed through FCT/MEC and co-financed by FEDER under the PT2020 Partnership Agreement. The NMR spectrometers are part of the National NMR Network (PTNMR) and are partially supported by Infrastructure Project 022161 (co-financed by FEDER through COMPETE 2020, POCI and PORL and FCT through PIDDAC). This work has received funding from the European Research Council (ERC) under the European Union's Horizon 2020 research and innovation program (grant agreement no. 865974). FCT is also acknowledged by R.B.L. Vieira and M. Ilkaeva for a Junior Researcher Position (CEECIND/02127/2017 and CEECIND/00546/2018, respectively), M. Sardo for an Assistant Research Position (CEECIND/00056/2020) and by J.M.P. Pereira for a PhD Studentship (SFRH/BD/145004/2019).

REFERENCES

(1) Masson-Delmotte, V.; Zhai, P.; Pörtner, H.-O.; Roberts, D.; Skea, J.; Shukla, P. R.; Pirani A.; Moufouma-Okia, W.; Péan, C.; Pidcock, R., et al. *IPCC, 2018: Global Warming of 1.5°C. An IPCC Special Report on the Impacts of Global Warming of 1.5°C above pre-industrial levels and related global greenhouse gas emission pathways, in the context of strengthening the global response to the threat of climate change, sustainable development, and efforts to eradicate poverty* **2018** In Press.

(2) Bhattacharyya, D.; Miller, D. C. Post-Combustion CO_2 Capture Technologies — a Review of Processes for Solvent-Based and Sorbent-Based CO_2 Capture. *Curr. Opin. Chem. Eng.* **2017**, *17*, 78–92.

(3) Zhao, X.; Cui, Q.; Wang, B.; Yan, X.; Singh, S.; Zhang, F.; Gao, X.; Li, Y. Recent Progress of Amine Modified Sorbents for Capturing CO_2 from Flue Gas. *Chinese J. Chem. Eng.* **2018**, *26* (11), 2292–2302.

(4) Modak, A.; Jana, S. Advancement in Porous Adsorbents for Post-Combustion CO_2 Capture. *Microporous Mesoporous Mater.* **2019**, *276*, 107–132.

(5) Aziz, B.; Hedin, N.; Bacsik, Z. Quantification of Chemisorption and Physisorption of Carbon Dioxide on Porous Silica Modified by Propylamines: Effect of Amine Density. *Microporous Mesoporous Mater.* **2012**, *159*, 42–49.

(6) Didas, S. A.; Sakwa-Novak, M. A.; Foo, G. S.; Sievers, C.; Jones, C. W. Effect of Amine Surface Coverage on the Co-Adsorption of CO_2 and Water: Spectral Deconvolution of Adsorbed Species. *J. Phys. Chem. Lett.* **2014**, *5*, 4194–400.

(7) Yu, J.; Chuang, S. S. C. The Structure of Adsorbed Species on Immobilized Amines in CO_2 Capture: An in Situ IR Study. *Energy & Fuels* **2016**, *30*, 7579–7587.

(8) Bacsik, Z.; Ahlsten, N.; Ziadi, A.; Zhao, G.; Garcia-Bennett, A. E.; Martín-Matute, B.; Hedin, N. Mechanisms and Kinetics for Sorption of CO_2 on Bicontinuous Mesoporous Silica Modified with *n*-Propylamine. *Langmuir* **2011**, 27, 11118–11128.

(9) Mafra, L.; Čendak, T.; Schneider, S.; Wiper, P. V.; Pires, J.; Gomes, J. R. B.; Pinto, M. L.

Structure of Chemisorbed CO_2 Species in Amine-Functionalized Mesoporous Silicas Studied by Solid-State NMR and Computer Modeling. *J. Am. Chem. Soc.* **2017**, *139*, 389–408.

(10) Mafra, L.; Čendak, T.; Schneider, S.; Wiper, P. V.; Pires, J.; Gomes, J. R. B.; Pinto, M. L. Amine Functionalized Porous Silica for CO_2/CH_4 Separation by Adsorption: Which Amine and Why. *Chem. Eng. J.* **2018**, *336*, 612–621.

(11) Čendak, T.; Sequeira, L.; Sardo, M.; Valente, A.; Pinto, M. L.; Mafra, L. Detecting Proton Transfer in CO_2 Species Chemisorbed on Amine-Modified Mesoporous Silicas by Using ^{13}C NMR Chemical Shift Anisotropy and Smart Control of Amine Surface Density. *Chem. - A Eur. J.* **2018**, *24*,10136–10145.

(12) Afonso, R.; Sardo, M.; Mafra, L.; Gomes, J. R. B. Unravelling the Structure of Chemisorbed CO_2 Species in Mesoporous Aminosilicas: A Critical Survey. *Environ. Sci. Technol.* **2019**, *53*, 2758–2767.

(13) Szego, A. E.; Jaworski, A.; Hedin, N. Chemisorption of CO_2 on Diaminated Silica as Bicarbonates and Different Types of Carbamate Ammonium Ion Pairs. *Mater. Adv.* **2021**, *2*, 448–454.

(14) Klinkenberg, N.; Kraft, S.; Polarz, S. Great Location: About Effects of Surface Bound Neighboring Groups for Passive and Active Fine-Tuning of CO_2 Adsorption Properties in Model Carbon Capture Materials. *Adv. Mater.* **2021**, *33*, 2007734.

(15) Heydari-Gorji, A.; Sayari, A. Thermal, Oxidative, and CO_2-Induced Degradation of Supported Polyethylenimine Adsorbents. *Ind. Eng. Chem. Res.* **2012**, *51*, 6887–6894.

(16) Sayari, A.; Belmabkhout, Y.; Da'na, E. CO_2 Deactivation of Supported Amines: Does the Nature of Amine Matter? *Langmuir* **2012**, *28*, 4241–4247.

(17) Jahandar Lashaki, M.; Khiavi, S.; Sayari, A. Stability of Amine-Functionalized CO_2 Adsorbents: A Multifaceted Puzzle. *Chem. Soc. Rev.* **2019**, *48*, 3320–3405.

(18) Qin, W.; Egolfopoulos, F. N.; Tsotsis, T. T. Fundamental and Environmental Aspects of Landfill Gas Utilization for Power Generation. *Chem. Eng. J.* **2001**, *82*, 157–172.

(19) D'Alessandro, D. M.; Smit, B.; Long, J. R. Carbon Dioxide Capture: Prospects for New Materials. *Angew. Chemie Int. Ed.* **2010**, *49*, 6058–6082.

(20) Tsai, W. T. Bioenergy from Landfill Gas (LFG) in Taiwan. *Renew. Sustain. Energy Rev.* **2007**, 11, 331–344.

(21) Choi, S.; Watanabe, T.; Bae, T.-H.; Sholl, D. S.; Jones, C. W. Modification of the Mg/DOBDC MOF with Amines to Enhance CO_2 Adsorption from Ultradilute Gases. *J. Phys. Chem. Lett.* **2012**, *3*, 1136–1141.

(22) Ghalei, B.; Sakurai, K.; Kinoshita, Y.; Wakimoto, K.; Isfahani, A. P.; Song, Q.; Doitomi, K.; Furukawa, S.; Hirao, H.; Kusuda, H.; Kitagawa, S., et al. Sivaniah, E. Enhanced Selectivity in Mixed Matrix Membranes for CO_2 Capture through Efficient Dispersion of Amine-Functionalized MOF Nanoparticles. *Nat. Energy* **2017**, *2*, 17086.

(23) Forse, A. C.; Milner, P. J.; Lee, J.-H.; Redfearn, H. N.; Oktawiec, J.; Siegelman, R. L.; Martell, J. D.; Dinakar, B.; Porter-Zasada, L. B.; Gonzalez, M. I.; Neaton, J. B.; Long, J. R.; Reimer, J. A. Elucidating CO_2 Chemisorption in Diamine-Appended Metal–Organic Frameworks. *J. Am. Chem. Soc.* **2018**, *140*, 18016–18031.

(24) Witherspoon, V. J.; Xu, J.; Reimer, J. A. Solid-State NMR Investigations of Carbon Dioxide Gas in Metal–Organic Frameworks: Insights into Molecular Motion and Adsorptive Behavior. *Chem. Rev.* **2018**, *118*, 10033–10048.

(25) Başaran, K.; Topçubaşı, B. U.; Davran-Candan, T. Theoretical Investigation of CO_2 Adsorption Mechanism over Amine-Functionalized Mesoporous Silica. *J. CO_2 Util.* **2021**, *47*, 101492.

(26) Chiang, W.-S.; Fratini, E.; Baglioni, P.; Georgi, D.; Chen, J.-H.; Liu, Y. Methane Adsorption in Model Mesoporous Material, SBA-15, Studied by Small-Angle Neutron Scattering. *J. Phys. Chem. C* **2016**, *120*, 4354–4363.

(27) Qajar, A.; Daigle, H.; Prodanović, M. The Effects of Pore Geometry on Adsorption Equilibrium in Shale Formations and Coal-Beds: Lattice Density Functional Theory Study. *Fuel* **2016**, *163*, 205–213.

(28) Hunger, M. Solid-State NMR Spectroscopy. *In Zeolite Chemistry and Catalysis*; Springer Netherlands: Dordrecht, **2009,** 65–105.

(29) Hunger, M. In Situ Flow MAS NMR Spectroscopy: State of the Art and Applications in Heterogeneous Catalysis. *Prog. Nucl. Magn. Reson. Spectrosc.* **2008**, *53*, 105–127.

(30) Massiot, D.; Fayon, F.; Capron, M.; King, I.; Le Calvé, S.; Alonso, B.; Durand, J.-O.; Bujoli, B.; Gan, Z.; Hoatson, G. Modelling One- and Two-Dimensional Solid-State NMR *Spectra. Magn. Reson. Chem.* **2002**, *40*, 70–76.

(31) McDonald, G. G.; Leigh, J. S. A New Method for Measuring Longitudinal Relaxation Times. *J. Magn. Reson.* **1973**, *9*, 358–362.

(32) Zhao, D.; Feng, J.; Huo, Q.; Melosh, N.; Fredrickson, G. H.; Chmelka, B. F.; Stucky, G. D. Triblock Copolymer Syntheses of Mesoporous Silica with Periodic 50 to 300 Angstrom Pores. *Science*. **1998**, *279*, 548–552.

(33) Thommes, M.; Kaneko, K.; Neimark, A. V.; Olivier, J. P.; Rodriguez-Reinoso, F.; Rouquerol, J.; Sing, K. S. W. Physisorption of Gases, with Special Reference to the Evaluation of Surface Area and Pore Size Distribution (IUPAC Technical Report). *Pure Appl. Chem.* **2015**, *87*, 1051–1069.

(34) Johnson, R. L.; Schmidt-Rohr, K. Quantitative Solid-State ^{13}C NMR with Signal Enhancement by Multiple Cross Polarization. *J. Magn. Reson.* **2014**, *239*, 44–49.

(35) Bernardinelli, O. D.; Lima, M. A.; Rezende, C. A.; Polikarpov, I.; DeAzevedo, E. R. Quantitative ^{13}C MultiCP Solid-State NMR as a Tool for Evaluation of Cellulose Crystallinity Index Measured Directly inside Sugarcane Biomass. *Biotechnol. Biofuels* **2015**, *8*, 110.

(36) Abragam, A. *The Principles of Nuclear Magnetism*; Clarendon Press: Oxford, United Kingdom **1961**.

(37) Paudel, A.; Geppi, M.; Mooter, G. Van den. Structural and Dynamic Properties of Amorphous Solid Dispersions: The Role of Solid-State Nuclear Magnetic Resonance Spectroscopy and Relaxometry. *J. Pharm. Sci.* **2014**, *103*, 2635–2662.

(38) Ciftja, A. F.; Hartono, A.; Svendsen, H. F. ^{13}C NMR as a Method Species Determination in CO_2 Absorbent Systems. *Int. J. Greenh. Gas Control* **2013**, 16, 224–232.

(39) Gul-E-Noor, F.; Michel, D.; Krautscheid, H.; Haase, J.; Bertmer, M. Investigation of the Spin-Lattice Relaxation of ^{13}CO and $^{13}CO_2$ Adsorbed in the Metal-Organic Frameworks $Cu_3(Btc)_2$ and $Cu_{3-x}Zn_x(Btc)_2$. *J. Chem. Phys.* **2013**, *139*, 034202.

(40) Etesse, P.; Zega, J. A.; Kobayashi, R. High Pressure Nuclear Magnetic Resonance Measurement of Spin–Lattice Relaxation and Self-diffusion in Carbon Dioxide. *J. Chem. Phys.* **1992**, *97*, 2022–2029.

(41) Sardo, M.; Afonso, R.; Juźków, J.; Pacheco, M.; Bordonhos, M.; Pinto, M. L.; Gomes, J. R. B.; Mafra, L. Unravelling Moisture-Induced CO_2 Chemisorption Mechanisms in Amine-Modified Sorbents at the Molecular Scale. *J. Mater. Chem. A* **2021,** *9***,** 5542–5555.

(42) Chiang, W.-S.; Fratini, E.; Baglioni, P.; Chen, J.-H.; Liu, Y. Pore Size Effect on Methane Adsorption in Mesoporous Silica Materials Studied by Small-Angle Neutron Scattering. *Langmuir* **2016**, *32*, 8849–8857.

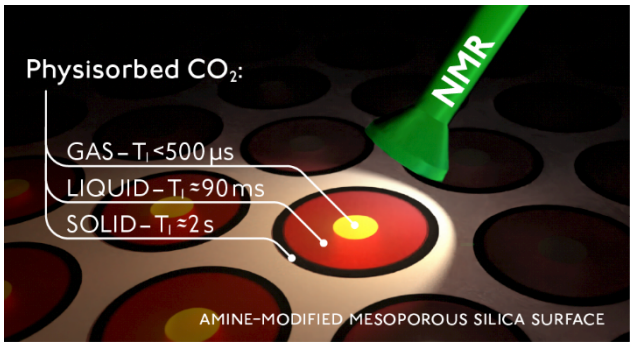
Physisorbed CO_2:
GAS – T_1 <500 µs
LIQUID – T_1 ≈90 ms
SOLID – T_1 ≈2 s
NMR
AMINE-MODIFIED MESOPOROUS SILICA SURFACE

TOC Graphic